

Article

Improvement of Thermal Protection in Recycled Polyolefins through Hybrid Mesoporous Silica–Antioxidant Particles

Enrique Blázquez-Blázquez ^{1,*}, Rosa Barranco-García ^{1,2}, Tamara M. Díez-Rodríguez ¹, Pilar Posadas ¹, Ernesto Pérez ¹ and María L. Cerrada ^{1,*}

¹ Instituto de Ciencia y Tecnología de Polímeros (ICTP-CSIC), Juan de la Cierva 3, 28006 Madrid, Spain; rbarranco@ictp.csic.es (R.B.-G.); t.diez@ictp.csic.es (T.M.D.-R.); pposadas@ictp.csic.es (P.P.); ernestop@ictp.csic.es (E.P.)

² Facultad de Ciencias Químicas, Universidad Complutense de Madrid, Avenida Complutense s/n, Ciudad Universitaria, 28040 Madrid, Spain

* Correspondence: enrique.blazquez@ictp.csic.es (E.B.-B.); mlcerrada@ictp.csic.es (M.L.C.)

Abstract: The deficient management of plastic waste has caused a serious worldwide environmental problem. Thus, one of the main challenges for the industry in the plastics sector in contributing to sustainability and a circular economy consists of providing a subsequent service life to this waste. For that purpose, the appropriate incorporation of antioxidants will play a key role in preventing or postponing the degradation of plastic waste, where the formation of radicals is initiated during its previous lifetime by the action of degrading agents. Functionalized particles, based on mesoporous MCM-41 silica with Irganox 1076, were prepared with two different protocols and were further incorporated into a material containing virgin PP and 30 wt.% of recycled PP, with the purpose of guaranteeing thermal stability during its next service life. A very significant increase in the thermal stability of the resulting composites was found, attributable to the synergistic action between the Irganox 1076 antioxidant and the MCM-41 particles. In addition, the presence of hybrid particles leads to an important nucleating effect for the crystallization of PP. Moreover, a reinforcing role was also played by these modified mesoporous silicas in the resultant systems. The presented methodology constitutes, therefore, a promising strategy for contributing to the circular economy—since the synergy between the Irganox 1076 antioxidant and MCM-41 particles was found to play an important role in the ultimate performance of recycled polyolefins.

Keywords: hybrid silica particles; mesoporous MCM-41; antioxidant; recycling; polyolefins; polypropylene



Citation: Blázquez-Blázquez, E.; Barranco-García, R.; Díez-Rodríguez, T.M.; Posadas, P.; Pérez, E.; Cerrada, M.L. Improvement of Thermal Protection in Recycled Polyolefins through Hybrid Mesoporous Silica–Antioxidant Particles. *Recycling* **2024**, *9*, 3. <https://doi.org/10.3390/recycling9010003>

Academic Editor: Denis Rodrigue

Received: 31 October 2023

Revised: 27 December 2023

Accepted: 29 December 2023

Published: 2 January 2024



Copyright: © 2024 by the authors. Licensee MDPI, Basel, Switzerland. This article is an open access article distributed under the terms and conditions of the Creative Commons Attribution (CC BY) license (<https://creativecommons.org/licenses/by/4.0/>).

1. Introduction

Our current era is marked by social consciousness about the environment and the imperative to reduce plastic waste. Thus, its recycling, in general, and that of polyolefins, in particular, has emerged as a pivotal step toward a sustainable future. Polypropylene (PP), a versatile and widely-used thermoplastic polyolefin, finds applications in a myriad of industries, from packaging to automotive components, many of them being single-use. Accordingly, this extensive use has led to the proliferation of discarded PP products, contributing significantly to the global crisis of plastic pollution. The mechanical recycling of PP involves plastic waste collection, cleaning it to remove impurities, shredding it into small pieces, and melting and reforming it into pellets, and other forms, so it can be employed for manufacturing new products. Proper recycling remains a major challenge because the necessary mechanical processing also promotes the degradation of thermoplastic polymers, resulting in a decrease in their mechanical and thermal properties, as well as a reduction in their subsequent service life [1,2]. This degradation process can be magnified by the presence of free radicals within the polymer chains, developed by their exposure to damaging agents such as heat, humidity, and the sun, among others, during their previous shelf

life. The absence of stabilizing agents during posterior processing can promote catalytic processes that will accelerate the propagation of these radicals [3,4].

Antioxidants are primarily used to prevent the accelerated oxidative degradation of polymers during their processing and their entire service life [5–8]. These stabilizers, which are preferentially located in amorphous polymeric phases, react in a free-radical based manner within polymeric macrochains either by attacking oxygen itself, or with the free radicals existing in the polymer chains. Antioxidants are commonly classified into primary and secondary ones [7]. The former act as hydrogen donors against peroxy radicals, and sterically hindered phenols are examples of this category. Conversely, secondary antioxidants are able to prevent the formation of free oxygen radicals. Organo-phosphite compounds are commonly used for this second type. A combination of both is frequently employed in polymers to provide much better comprehensive protection against thermal and oxidative degradation.

Most of these additives are organic compounds of relatively low molecular weight (<1200 g/mol) and are added in a small amount (below 1% by weight in most cases). Antioxidants are mixed together with the polymeric resins during processing and are required for the optimization of formulations to ensure their dispersion and long-term effectiveness within the matrix. Irganox 1076[®] is one of the most common phenolic antioxidant used. Its effectiveness can be conditioned by: compatibility with the polymer matrix, the amount incorporated, and the formation of crystals or their migration to the surface, among other variables [9–11].

Furthermore, different inorganic compounds, based on aluminosilicate clay minerals or silica particles, have been used as carriers of antioxidants to maximize their efficiency, leading to the improvement of the thermo-oxidative behavior of elastomers and thermoplastics [12–15]. Thus, materials based on mesoporous silica, such as SBA-15 (Santa Barbara Amorphous) or MCM-41 (Mobil Crystalline Materials No. 41), have been explored as adsorbers of different bioactive polyphenols from red wine [16], as carriers of small antioxidant molecules, gallic acid [17] for instance, and have also been analyzed regarding the prolonged release of other substances [18,19]. Their adsorption ability is mainly due to a homogenous hexagonal channel structure within an ordered mesoporous arrangement, large pore volume, a large surface area, and excellent chemical and thermal stability [20].

The aim of this study was to incorporate hybrid particles based on mesoporous MCM-41 silica and Irganox 1076 into recycled polyolefins in order to improve their thermal stability. Accordingly, model blends of virgin PP with 30% by weight of recycled PP were melt extruded, adding neat Irganox 1076 (0.5 wt.% related to that of the polymeric fraction) or hybrid MCM-41@Irganox 1076 particles, where Irganox 1076 is the minor component, as antioxidants. Modified mesoporous silica was obtained with two different approaches: (a) via direct contact through the sonication of both types of solid particles (MCM-41 and Irganox 1076); and (b) by dissolving Irganox 1076 in dichloromethane (wet impregnation method) and adding this solution to the MCM-41 silica and enabling the complete evaporation of the solvent. Once the different antioxidants were prepared, their detailed characterization was carried out, as was the characterization of the various recycled materials. Several techniques were used—nitrogen adsorption/desorption, X-ray diffraction with synchrotron radiation, gas chromatography coupled to mass spectrometry (GC/MS), differential scanning calorimetry (DSC), oxidation induction time (OIT) tests, thermogravimetry (TGA), and microhardness (MH) measurements—in order to analyze the thermal stability of the resulting composites, and their crystallization ability, and a preliminary analysis of their mechanical performance. The main novelty of the present research is based on the investigation of the use, for the first time in the field of polymer recycling, of mesoporous MCM-41 particles as carriers of antioxidants, which constitutes a highly efficient method for introducing antioxidants in polyolefin matrixes. This methodology would allow the possibility of reducing the amount of antioxidants needed during the production processes, which impacts favorably on the overall sustainability.

2. Results and Discussion

2.1. Characterization of Modified Particles

Mesoporous MCM-41 silica has been decorated with the Irganox 1076 antioxidant using two protocols, as just commented on in the Introduction and specified in the Section 3. Thus, hybrid MCM-41@Irganox 1076 particles were obtained by direct contact using ultrasound or prepared from a previous Irganox 1076 solution, labeled as MCMA and MCMAD, respectively. Their characterization shows some differences and analogies between them. Figure 1 shows the wide-angle X-ray scattering (WAXS) profiles obtained using synchrotron radiation at three different temperatures (20, 35, and 56 °C) during a heating experiment at 20 °C/min of these hybrid mesoporous particles. The pure antioxidant Irganox 1076 is characterized by its high crystallinity, showing numerous sharp diffractions in its WAXS pattern, and melts at about 55 °C. Its melting behavior as well as its polymorphism has been widely studied [9]. Figure 1 indicates important differences between MCMA and MCMAD particles. Thus, the profiles at 20 and 35 °C in the former are composed of an amorphous halo, arising from the silica and involving a large area, overlapped with several reflections of much smaller intensity, while only the halo is observed in the pattern at 56 °C. In contrast, the diffractograms at the different temperatures for the MCMAD silica show that these particles are completely amorphous. Direct contact between MCM-41 silica and Irganox 1076 using ultrasound (MCMA particles) might promote interactions between the silanol groups existing on the external surface of MCM-41 with the hydroxyl and ester groups from the Irganox 1076. Nevertheless, those physical links do not alter the short-term amorphous nature of this mesoporous silica [20] and the crystalline structure of the antioxidant. Thus, both components appear in the profiles at low temperatures, with the one corresponding to the silica being of much higher intensity because it is the major constituent in the hybrid particles. At 56 °C, which is a temperature above the melting of Irganox 1076, both components are in a disordered state and only an overall amorphous halo is visible.

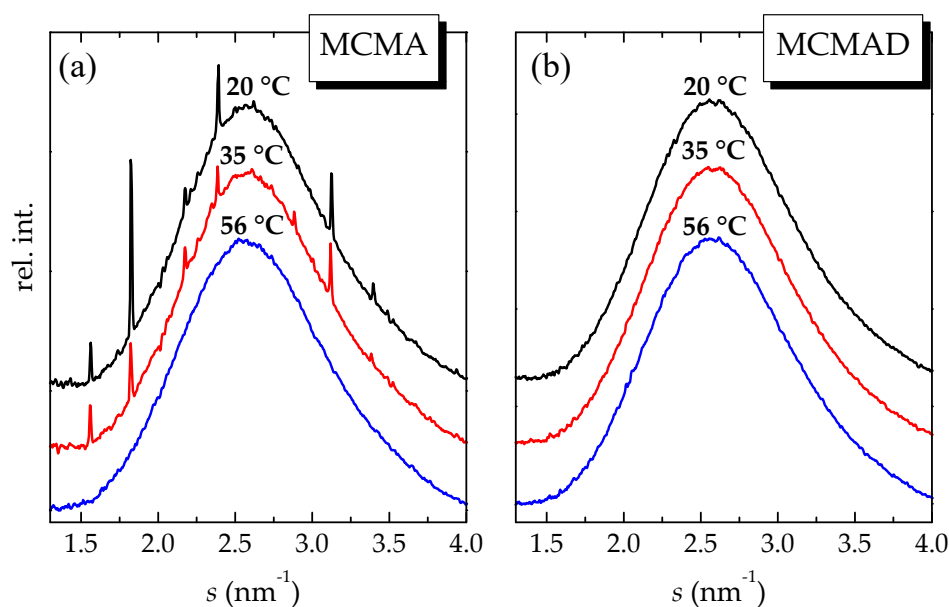


Figure 1. Synchrotron WAXS patterns of the hybrid MCM-41@Irganox 1076 particles at different temperatures obtained during a heating experiment at 20 °C/min: (a) MCMA and (b) MCMAD.

On the other hand, the incorporation of Irganox 1076 into MCM-41 through the wet impregnation method, leading to the MCMAD particles, was carried out from the solution of the antioxidant in dichloromethane followed by its complete drying. This protocol seems to hinder the crystallization of the antioxidant during solvent evaporation and, consequently, the WAXS profiles show only an amorphous halo for the hybrid MCMAD

silica, regardless of the temperature analyzed, as deduced from Figure 1b. This approach appears to boost stronger interactions between the mesoporous MCM-41 and the Irganox 1076, preventing the crystallization of the latest. In fact, this modification route can enable the insertion of Irganox 1076 solution within the empty mesostructure of MCM-41, inducing a more intimate internal contact between silica and antioxidant, in addition to the interactions between the antioxidant and the silanol groups on the external surface of the silica. The inclusion of low-molecular-weight substances in the nanometric pores of the mesoporous silica is described in the literature [21,22], along with the incorporation of segments of macromolecular chains [23–25] or metals like silver [26,27], leading to their confinement [28,29]. This capability of mesoporous silica for the amorphization of antioxidants and poorly soluble drugs is a feature already reported [30–32].

The SEM micrographs (Figure 2) of MCMA and MCMAD particles also display their differences depending on the modification route. Neat MCM-41 silica is characterized by an irregular micrometric shape [33,34] and no significant changes have been found between that synthesized in the laboratory and the commercial ones. Thus, MCMA is constituted of individual MCM-41 particles as a major component where spherical Irganox 1076 ones are deposited. Consequently, the two solids are clearly observed. However, the image for MCMAD depicts a superficial continuity which is much more significant, although single antioxidant particles are also distinguishable between the two components of the hybrid silica. This feature is due to the more intimate contact promoted during the application of the wet impregnation methodology used for its preparation.

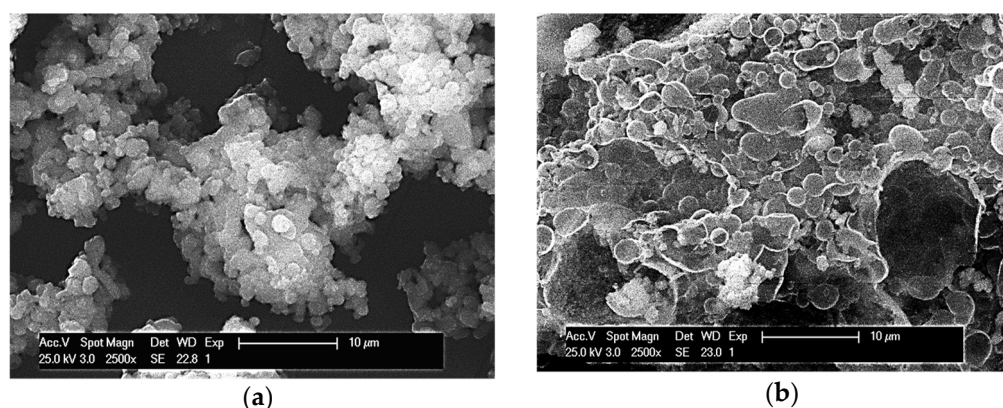


Figure 2. SEM images of the hybrid MCM-41@Irganox 1076 particles: (a) MCMA and (b) MCMAD.

Other very interesting characteristics for mesoporous silicas are deduced from the N_2 adsorption–desorption measurements, whose results are represented in Figure 3a for pristine MCM-41 and the hybrid MCMA and MCMAD particles together with those for pore volume analysis depicted in Figure 3b. On one hand, the different neat or modified particles show a reversible type IV isotherm, indicating the existence of mesoporosity, with a hysteresis loop Type H1, which is characteristic for pore-expanded mesoporous silica with a high degree of pore size uniformity, according to the IUPAC classification [35,36]. However, the amount of N_2 adsorbed on functionalized particles diminishes when compared with that attained for the pure MCM-41, being quite analogous for the two decorated MCM-41@Irganox 1076, pointing out a reduction in pore volume owing to the surface modification of the silica. Thus, the specific surface area, calculated on the basis of Brunauer–Emmett–Teller (BET) theory, shows a value of $908 \text{ m}^2/\text{g}$ for the bare MCM-41 while it decreases to 857 and 848 for MCMA and MCMAD, respectively. As seen in Figure 3b, the pore width also moves to lower values in the modified particles, changing the diameter from 2.65 nm to 2.51 nm and to 2.50 nm for MCM-41, MCMA, and MCMAD, respectively, as determined by BJH adsorption analysis. Lower values for surface area and pore diameter can be associated with a partial insertion of the antioxidant within the mesopores of the silica [16], being slightly larger in the particles functionalized by means of the wet impregnation protocol.

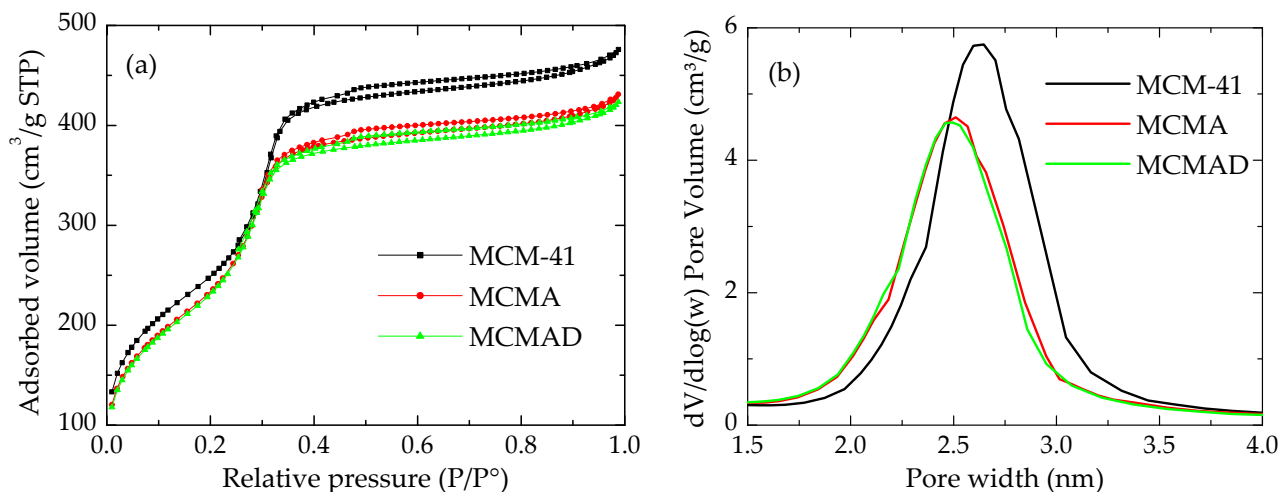


Figure 3. (a) N₂ adsorption–desorption isotherms for the pristine MCM-41 and the MCMA and MCMAD hybrid particles. (b) Pore size distribution of the particles determined using the model proposed by Barrett–Joyner–Halenda, BJH.

2.2. Characterization and Properties of the Different Materials

The phase transitions related to the crystalline characteristics of the different materials analyzed, both the pure components and the different systems with Irganox 1076, have been evaluated by differential scanning calorimetry (DSC). They are the virgin PP, the recycled PP (PPR), the material named as PP73 (containing virgin PP with a 30 wt.% of recycled PP without any additional additive), the material labeled as PP73A (based on PP73 with a small amount of the Irganox 1076 antioxidant), the material designated as PP73AD (based on PP73 and a small content of Irganox 1076, which was incorporated by dissolving it in dichloromethane before extrusion), and for the materials designated as PP73AM and PP73AMD (both based on PP73 with Irganox 1076 and silica MCM-41. A solid contact between Irganox 1076 and mesoporous MCM-41 was carried out in the former, while Irganox 1076 was embedded in MCM-41 using its wet impregnation with dichloromethane for the latter). Table 1 lists the nominal content in each constituent. More details can be found in the Materials and Methods.

Table 1. Nominal composition of the different systems in weight percentage (wt.%) of each component, maintaining as constant the ratio of 70:30 between virgin PP/PPR in the binary and ternary materials.

Sample Name	Polymer Composition		Irganox 1076	Irganox 1076D	MCMA	MCMAD
	PP070	PPR				
Virgin PP	100					
PPR		100				
PP73	70	30				
PP73A	69.6	29.9	0.5			
PP73AD	69.6	29.9		0.5		
PP73AM	63	27			10	
PP73AMD	63	27				10

Figure 4 shows the DSC curves obtained during the first heating cycle at a rate of 20 °C/min. A single melting process is noticed in the curve for the virgin PP, which is located at about 165 °C, while two endothermic events are exhibited by the PPR, at around 160 °C and 128 °C, respectively. The existence of these two meltings indicates that PPR is not a bare recycled PP, but rather it contains a fraction of polyethylene (PE) from cross contamination [37,38]. Thus, the peak at the highest temperatures is related to the polypropylene component in PPR, which might be composed, due to its recycled nature, of a mixture of different grades including homopolymers and copolymers, while the peak at

low temperature is attributed to PE. The calculated amount of PE in PPR, according to the literature [39], is around 22 wt.%. As expected, the fraction of PE is considerably reduced (and, consequently the area of its melting process) in the PP73 material and its derivatives with Irganox 1076. The melting temperature (T_m) corresponding to the crystallites of the PP component is located in these PP73-based systems in between those from virgin PP and PPR. Differences in intensity are due to the fact that these DSC curves are not normalized to the actual amount of PP, not due to significant differences in the degree of crystallinity.

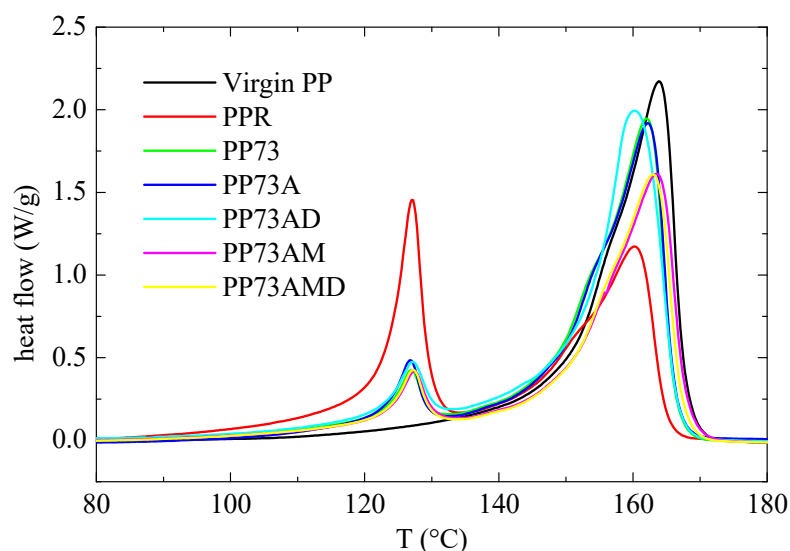


Figure 4. DSC curves obtained from the first heating run at a rate of 20 °C/min for the bare PP, the recycled PPR, and the different PP73 materials based on their mixing without or with additional Irganox 1076.

Figure 5 displays, for all the different systems, the cooling process carried out at two different rates: 20 and 2 °C/min, in order to understand how the addition of PPR and the incorporation of the Irganox 1076 antioxidant by several approaches (including those involving the use of MCM-41 silica) influenced the crystallization of the resultant materials. At a cooling rate of 20 °C/min, virgin PP crystallized at around 117.5 °C, while PPR showed an exotherm with two overlapped processes, being the low-temperature shoulder associated with the crystallization of its PE fraction. Contrary to the behavior noted during melting, all the PP73-based materials exhibited their crystallization temperature (T_c) (defined as the temperature in the minimum) at considerably higher temperatures than those T_c s for virgin PP and PPR, as shown in Figure 5a. This displacement is even more significant for the PP73AM and PP73AMD systems because of the incorporation of MCM-41 particles that play a nucleating role. The opposite feature has been previously described in other PP composites prepared by extrusion [40], i.e., the PP crystallization was postponed, so that MCM-41 particles delayed the three-dimensional ordering process. A mixed effect has been also reported depending on the MCM-41 characteristics [41]. This different behavior can be associated with the distinct microstructural details of the PP matrices under study and also with the synthetic method of the mesoporous silica. The type of polymer is also important, and a significant nucleating effect of MCM-41 has been observed for the PLA crystallization in its composites with this mesoporous silica [42,43].

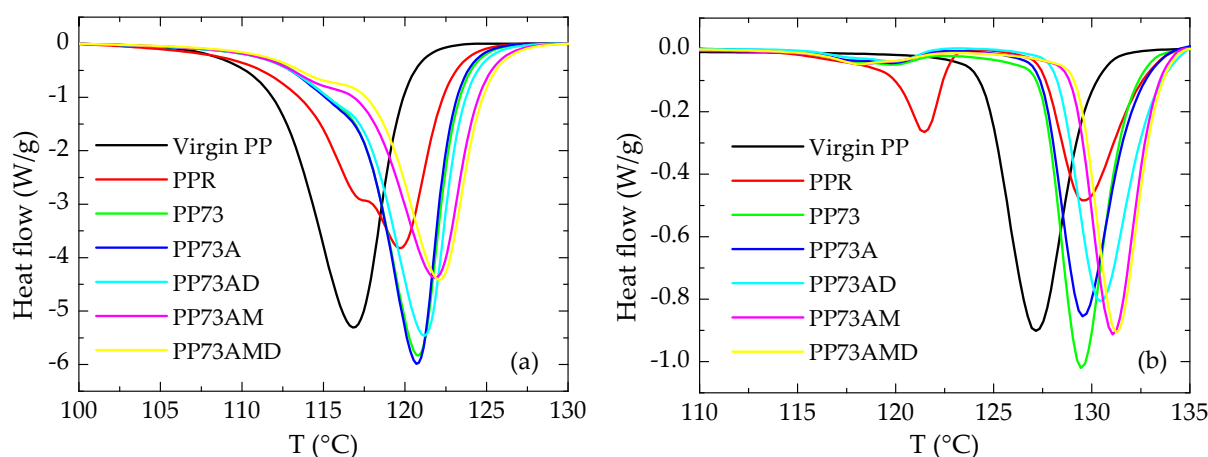


Figure 5. DSC cooling curves from the melt for the bare PP, the recycled PPR, and the different PP73 materials based on their mixing without or with additional Irganox 1076: (a) at a rate of 20 °C/min and (b) at a rate of 2 °C/min.

Figure 5b shows cooling results achieved at a rate of 2 °C/min. As expected, all crystallization processes are shifted to higher temperatures because of the more favorable conditions applied during cooling. In addition, the crystallization of PE and PP fractions are now well separated in the PPR material. A very analogous location for T_c is also observed in PPR (for its PP fraction), PP73, and PP73A, shifting slightly to a higher temperature in PP73AD. Again, the influence of MCM-41's presence as a nucleant leads to a greater shift of crystallization to higher temperatures in PP73AM and PP73AMD.

In order to obtain deeper knowledge, a study of isothermal crystallization at different temperatures has been performed. Figure 6a represents the results obtained for PP73, PP73A, and PP73AM. It is clearly evident that the isothermal crystallization at all of the studied temperatures is rather analogous for PP73 and PP73A, but significant differences with the PP73AM system are observed. These results seem to indicate that the incorporation of a small amount of Irganox 1076 as an antioxidant in PP73A does not affect the crystallization of PP. However, this ordering process is strongly dependent on the presence of MCM-41, which acts as a nucleating agent, as noticed from the dynamic cooling experiments. Thus, crystallization requires shorter times to take place.

Figure 6b summarizes the variation with isothermal crystallization temperature of the time at which the exotherm reaches the minimum for all of the materials. A significant difference is noted between virgin PP and PPR. Thus, PPR crystallizes faster than the former. This fact can be attributed to the different microstructural and molecular characteristics of these two PP polymers; it is important to recall that the PP constituent in PPR can be composed by distinct grades of PP homopolymers and copolymers, in addition to the presence of a PE fraction and of oxidative species. The remarkable feature of Figure 6b is the great influence that PPR plays on the crystallization of the PP73 resulting systems despite PPR representing the minor component, being added at 30 wt.%. Thus, the dependence of t_{peak} on the isothermal crystallization temperature is very similar for PPR, PP73, PP73A, and PP73AD. However, crystallization occurs faster when hybrid MCM-41@Irganox 1076 particles are added, independently of the protocol for its preparation.

Another important aspect to analyze in recycled polymeric materials is their mechanical response to know if a significant variation has occurred due to the presence of recycled content. As mentioned above, the materials examined here incorporate an intermediate amount (30 wt.%) of recycled PP. For a preliminary evaluation, the determination of microhardness (MH) has been chosen. Figure 7 shows that virgin PP exhibits higher MH values than PPR, while the MH for the PP73-based materials lies between these two extremes. The lower values found in the PPR can be associated with its greater molecular heterogeneity, where a soft fraction of PE [44], as well as the existence of oxidative species, caused during

its previous useful life, affect the size of PP crystallites, as deduced from its lower T_m compared with that presented by the virgin PP. Furthermore, it should be kept in mind that it might be constituted by different grades of PP homopolymers and copolymers with different compositions and the latter exhibit a reduction in crystallinity, crystal size, and mechanical parameters ascribed to rigidity [45,46], as is MH.

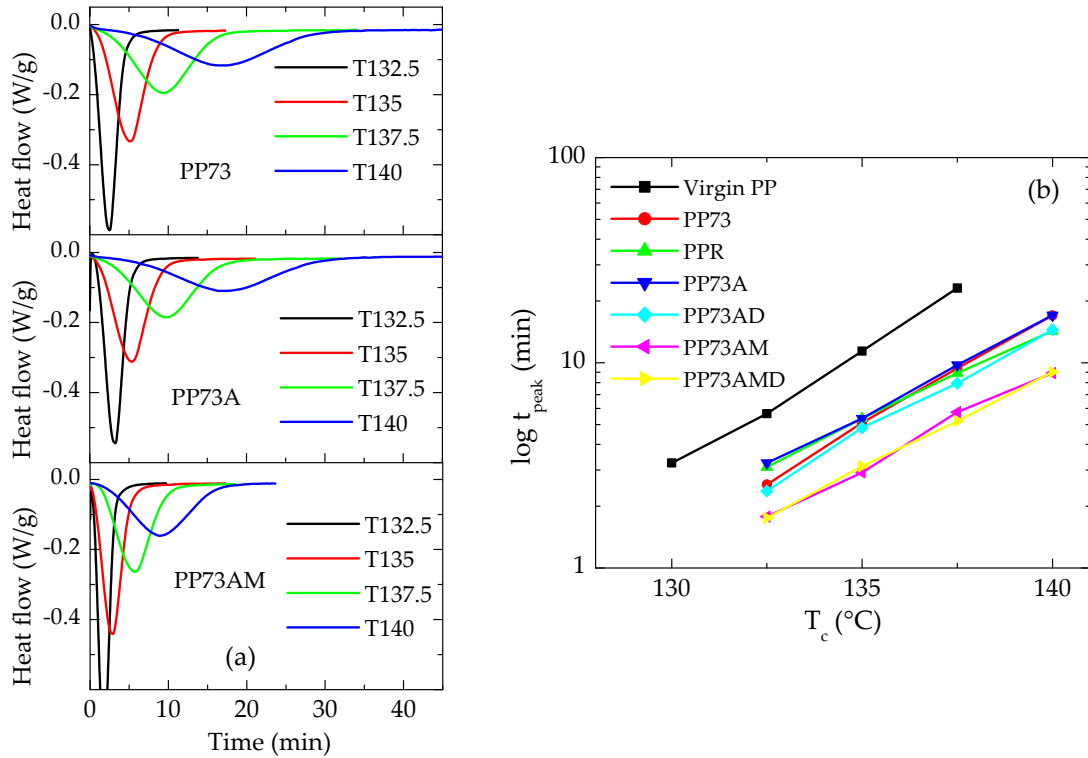


Figure 6. (a) Results for isothermal crystallization experiments at different temperatures for the PP73 materials without and with Irganox 1076: PP73, PP73A, and PP73AMD (from top to bottom). (b) Dependence of time (on logarithmic scale) at which the exotherm reaches the minimum isothermal crystallization temperature for all of the materials.

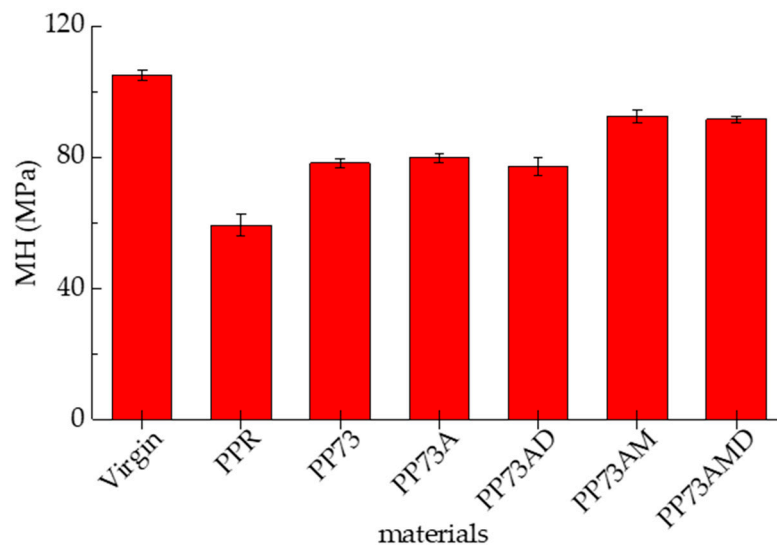


Figure 7. Microhardness values for the different materials analyzed, showing the standard deviation of the five different measurements.

Concerning the PP73-based systems, the results indicate that incorporation of only Irganox 1076, independently of the method followed, does not affect the stiffness of the final materials. Thus, the MH values are quite analogous for PP73, PP73A, and PP73AD. On the contrary, MH increases considerably (and consequently the rigidity) in the systems where the addition of antioxidant is assisted by MCM-41, this increase also being independent of the preparation protocol of the hybrid particles. Therefore, MCM-41 also plays a role as a reinforcement agent [25,47], with higher MH values in PP73AM and PP73AMD compared with that of PP73.

Another aspect of great importance in recycled polymeric materials is the knowledge of their final thermal stability. For this, thermogravimetric analyses have been carried out. Figure 8 shows the values of the temperature at a weight loss of 5% ($T_{5\%}$) for the different materials, deduced from their thermogravimetric curves carried out under a nitrogen atmosphere. As can clearly be seen, the lowest temperature is found in the virgin PP. Thus, the incorporation of a 30 wt.% of PPR improves the thermal stability in the sample PP73, moving the $T_{5\%}$ more than 10 °C towards higher temperatures. The greater $T_{5\%}$ value found in PPR could be associated with the presence of a PE fraction, since the higher degradation temperature of PE compared to that for PP is well-known [48]. The incorporation of a small amount of Irganox 1076 implies an additional increase in $T_{5\%}$ when comparing values between PP73 and PP73A, while the increase is much more significant, above 30 °C, when the addition is performed either by the methodology of wet impregnation of the single antioxidant, i.e., in PP73AD, or when Irganox 1076 is added together with MCM-41. This behavior is rather interesting since it has been reported that neat MCM-41 has a catalytic effect in the degradation process of some polymers, such as PE, for example [23,49]. The importance of specific functionalization depending on the intended final application is, therefore, evident.

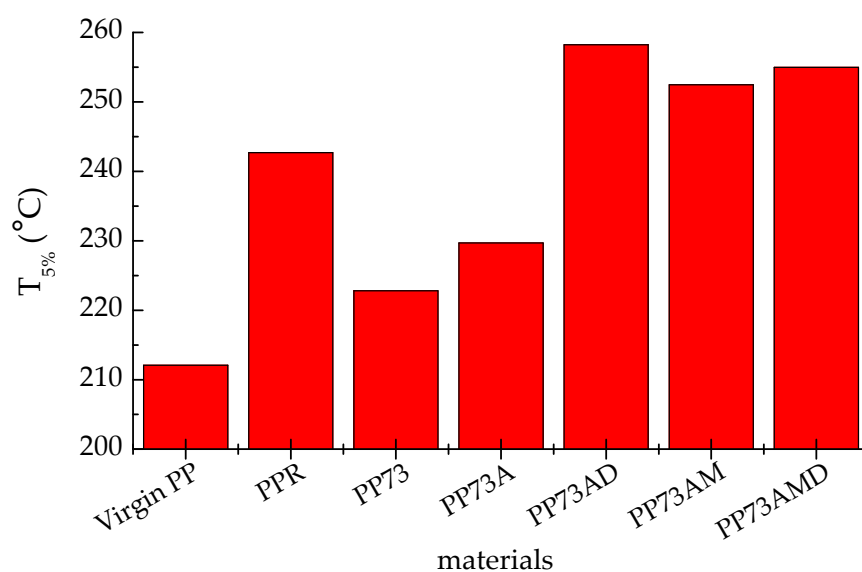


Figure 8. $T_{5\%}$ values obtained from the TGA curves performed at a rate of 10 °C/min under an inert environment for the different materials analyzed.

Additional kinetic thermogravimetric experiments have been performed on these three materials with the highest $T_{5\%}$ values at different heating rates: 2, 5, 10, and 20 °C/min under nitrogen and oxygen atmospheres, whose results are represented in Figure 9. The temperatures for the maximum degradation rate, calculated at the minimum of the derivative curves, are noticeably lower in the experiments carried out in oxygen than in those performed in nitrogen, as expected. Furthermore, the results under an oxygen atmosphere are similar for the three materials. On the contrary, measurements under a nitrogen atmosphere show a shift of approximately 8 °C in the degradation temperature for those systems

containing hybrid MCM-41 particles. This response could be attributed to a better stability of PP73AM and PP73AMD materials when the degradation is extended through their bulk. These results agree with those previously described [50], where an effective delay was observed in the build-up of distinctive species, involving a higher thermal stability, although the degradation mechanism did not change in the presence of mesoporous silica.

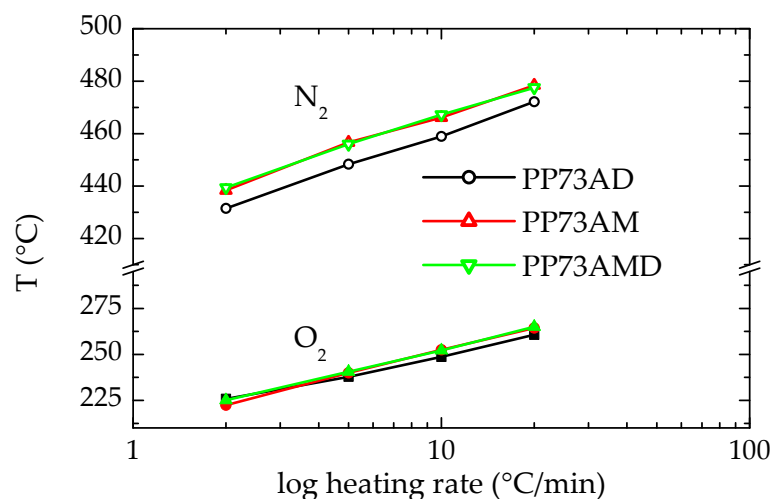


Figure 9. Temperature for the maximum degradation rate in TGA experiments at 2, 5, 10, and 20 °C/min under an inert and oxidative atmosphere.

In order to fully understand the overall thermal stability of all of the recycled systems, a detailed study of the presence of other antioxidants, different than the added Irganox 1076, is mandatory. As discussed in the introduction, secondary antioxidants are commonly added to polymeric materials to prevent their degradation during processing, since they hinder the formation and incorporation of oxygen-containing radical species into the polymeric macrochains. Figure 10 shows the gas chromatograms (GC) for the virgin PP and PPR, in which the presence of two peaks located at the same retention time is observed, although with different intensity for both. The one located at about 24.2 min corresponds to Irganox 168, whose amount is very low in PPR. The peak at around 25.6 min is ascribed to the oxidized form of Irganox 168, being much more intense in PPR than in the virgin PP. Irganox 168 is a secondary antioxidant, composed of phosphite groups that can undergo oxidation to phosphate ones during processing at elevated temperatures or when the polymers are exposed to sunlight or humidity [51–53].

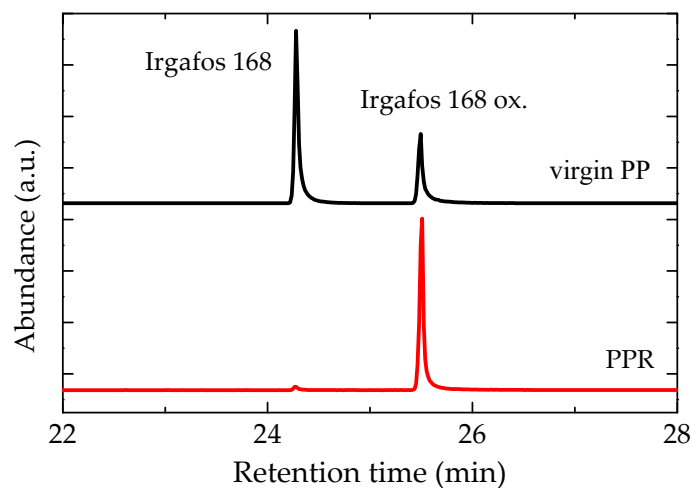


Figure 10. Gas chromatograms obtained for the analysis of the additive content in virgin and recycled polypropylene.

A valuable tool to elucidate the advance of degradation in polymers is to calculate the ratio between both species: Irgafos 168 and oxidized Irgafos 168. A low value of this ratio is associated with a massive consumption of the antioxidant. The estimated ratios for these materials are listed in Table 2. The ratio for virgin PP after its extrusion is greater than 2, indicating that the antioxidant groups of Irgafos 168 are the main species. On the contrary, this value is drastically reduced for extruded PPR, and the amount of pristine Irgafos 168 in the PP73 blend is also very low. In order to evaluate the results derived from the melt extrusion, knowledge of this parameter is necessary for the starting pellets of virgin PP and of PPR. Determination was performed following the same extraction protocol described in the Materials and Methods, and the ratio found between both species was 2.90 for the virgin PP and 2.27 for PPR. These results indicate, on one hand, that both pellets incorporated a rather equivalent content of Irgafos 168 and, on the other hand, that there was a massive consumption of Irgafos 168 during the extrusion of PPR, which is attributed to the existence of a high content of oxidative species, whose activity grows exponentially during processing at high temperatures under an air atmosphere [3]. In the rest of the systems, an additional content of the primary antioxidant Irganox 1076 was added following distinct procedures, and a completely different response was observed. It not only acted during the useful life but also demonstrated its effectiveness during this new processing by extrusion, allowing a reduction in the consumption of Irgafos 168. This result is even better in the case of using hybrid MCM-41@antioxidant particles, suggesting a synergistic action between antioxidant and mesoporous particles.

Table 2. Calculated ratios of Irgafos 168 and its oxidized form.

Material	Ratio Irgafos 168/ Irgafos 168 Ox.
Virgin PP	2.02
PPR	0.02
PP73	0.14
PP73A	0.59
PP73AD	2.20
PP73AM	1.86
PP73AMD	2.61

In order to estimate the global antioxidant activity in the blends, tests for determining the oxidation induction time [54,55] have been also performed. Figure 11 represents the DSC curves obtained after switching the purge gas from nitrogen to oxygen at 180 °C, which was the temperature that was kept constant during rest of the experiment. The results indicate a low OIT value for the virgin PP and for the PP73 blend, which did not contain any additional antioxidants. This result could be contradictory with the presence of a significant amount of Irgafos 168 in the pure materials virgin PP and PPR. Nevertheless, Irgafos 168 scarcely contributes to the improvement of OIT values, because it is rapidly converted into its oxidized product in the presence of oxygen [51]. In contrast, the addition of a primary antioxidant, such as Irganox 1076, notably improves the protection of the systems, and the OIT values increase from 2 to 47 min in PP73A. The behavior of the material to which the antioxidant Irganox 1076 has been added through wet impregnation with dichloromethane is notable. Favorable dispersion and stronger interactions within the polymer chains might provide a better and homogeneous protection ability, leading to an OIT value of 109 min in PP73AD. Even higher OIT values are obtained for the materials containing the hybrid MCM-41@Irganox 1076 particles, with the PP73AMD system showing the best response. Furthermore, a different shape of the curve is also noticed in the materials with silica particles. The strong adsorption of the Irganox 1076 antioxidant on the external and internal surfaces of silica could hinder its migration, so that the degradation occurs less abruptly and is delayed in time [13].

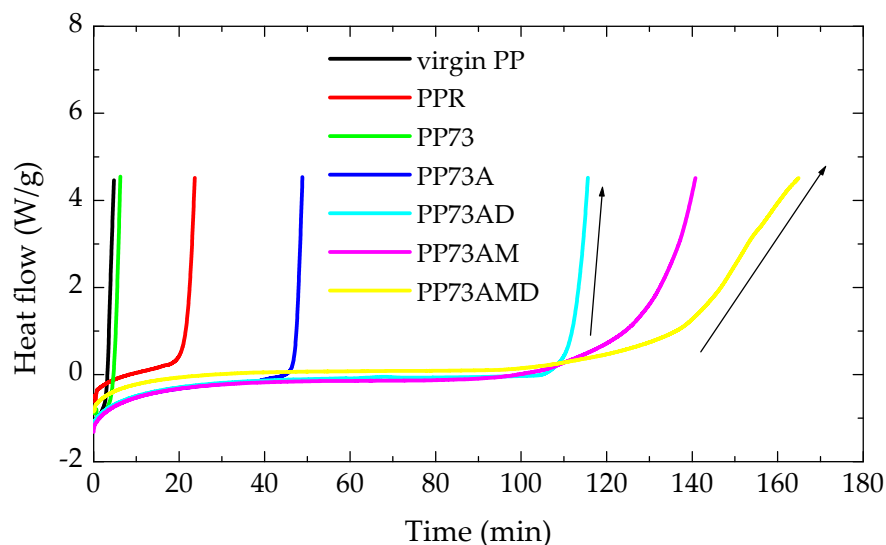


Figure 11. Heat flow curves for determination of OIT values in the different materials analyzed at an isothermal temperature of 180 °C.

3. Materials and Methods

3.1. Materials and Chemicals

A commercially available Ziegler-Natta catalyzed isotactic polypropylene, identified as PP070 (supplied by Repsol, Sigma-Aldrich Madrid, Spain), with a melt flow index of 12 g/10 min (230 °C, 2.16 kg, ISO 1133) together with a post-consumer recycled polypropylene, labeled as PPR (supplied by Armando Álvarez Group, Torrelavega, Spain), with a melt flow index of 4.1 g/10 min (230 °C, 2.16 kg, ISO 1133) have been used in this study.

Pristine mesoporous MCM-41 silica was purchased from Sigma-Aldrich (St. Louis, MO, USA), and Irganox 1076® (CAS 2082-79-3) was supplied by Sigma-Aldrich. Dichloromethane (>99.9%, Honeywell) was employed as a solvent for extraction processes and for the obtainment of the hybrid mesoporous silica.

3.2. Preparation of Hybrid MCM-41@Irganox 1076 Particles

To proceed with the functionalization of mesoporous MCM-14 particles, which were previously dried at 100 °C for 4 h, two different protocols were followed: (a) the solid contact between particles promoted by ultrasounds [56] and (b) the wet impregnation method. In the former, 28 mg of Irganox 1076 was contacted with 550 mg of MCM-41 by mixing using an ultrasound bath for 15 min. These particles were named as MCMA. And (b) 28 mg of Irganox 1076 was firstly dissolved in 4 mL of dichloromethane before their mixing with MCM-41 for 15 min in an ultrasonic bath. Then, the solvent was removed at room temperature until dryness. These particles have been designated as MCMAD. The amounts of MCM-41 and Irganox 1076 were calculated in order to reach a final content of 10 wt.% and 0.5 wt.% by weight, respectively, in the final recycled material.

3.3. Preparation of Materials and Processing of Films

Firstly, a material based on virgin and recycled polypropylene, containing a proportion of 70:30 % by weight, respectively, named as PP73, was prepared by melt extrusion at 190 °C and 100 rpm for 5 min in a Haake Minilab twin-screw extruder (Thermo Electron Corporation, Waltham, MA, US) with a volumetric capacity of 7 cm³, using co-rotating conical screws. These two systems, virgin and recycled PP, labeled as Virgin and PPR, were also extruded individually under identical conditions to fully understand the influence that the incorporation of PPR has in the physical-chemical characteristics of the Virgin matrix. Furthermore, the Irganox 1076 antioxidant was added into the Virgin and PPR pellets before their joint extrusion following two different protocols: (a) simply by manual mixing and stirring (designated as PP73A) and (b) by incorporation of a solution constituted by

the antioxidant in a small amount of dichloromethane (called as PP73AD). Finally, ternary composites based on Virgin, PPR, and hybrid MCM-41@Irganox 1076 particles (using either MCMA or MCMAD silicas) were obtained using the extrusion protocol aforementioned for the preparation of the PP73 material. Table 1 describes in detail the compositions of all the systems under study.

Extrudates of the different materials were processed as films by compression molding in a Collin press between hot plates at 190 °C for 4 min, applying a pressure of 25 MPa. Next, fast cooling was applied from 190 °C down to ambient temperature between steel plates refrigerated with water (average cooling rate around 80 °C/min). The thickness of these films ranged from 0.18 to 0.22 mm.

3.4. Characterization of the Hybrid MCM-41@Irganox 1076 Particles

3.4.1. X-ray Experiments with Synchrotron Radiation

Real-time variable-temperature WAXS experiments were carried out with synchrotron radiation in a beamline BL11-NCD-Sweet at ALBA (Cerdanyola del Vallès, Barcelona, Spain) at a fixed wavelength of 0.1 nm. A Rayonix detector was used at a distance about 19 cm from sample and a tilt angle of around 30°. A Linkam Unit, connected to a cooling system of liquid nitrogen, was employed for the temperature control. The calibration of spacings was obtained by means of silver behenate and Cr₂O₃ standards. The initial 2D X-ray images were converted into 1D diffractograms, as a function of the inverse scattering vector, $s = 1/d = 2 \sin \theta / \lambda$. The different types of particles as powders were enveloped in aluminum foil for their WAXS analysis.

3.4.2. Scanning Electronic Microscopy

Hybrid particles were examined by scanning electron microscopy (SEM) using a Philips XL30 microscope (F.E.I. Company, Hillsboro, OR, USA). The samples were coated with a layer of 80:20 Au/Pd alloy and deposited in a holder before visualization.

3.4.3. N₂ Adsorption/Desorption

Different parameters, such as specific surface area, pore volume, or pore size, were estimated by nitrogen adsorption/desorption isotherms at −196 °C with an Asap 2420 Micromeritics instrument (Norcross, GA, USA). Prior to the adsorption measurements, the sample was outgassed under vacuum for 10 h at 300 °C. The BET specific surface area was calculated in the relative pressure range of 0.06–0.19. The pore volume was determined at the relative pressure of 0.98. The pore size distribution was assessed from the desorption branch of the N₂ adsorption isotherms using the model proposed by Barrett–Joyner–Halenda, BJH.

3.5. Characterization of the Films

3.5.1. Differential Scanning Calorimetry

Calorimetric analyses were carried out in a TA Instruments Q100 calorimeter connected to a cooling system and calibrated with different standards. The sample weights were around 5 mg. A temperature interval from 20 to 190 °C was studied at a heating/cooling rate of 10 °C/min.

3.5.2. Microhardness

A Vickers indenter attached to a Leitz microhardness tester was used to perform microindentation measurements undertaken at 23 °C. A contact load of 0.98 N for 30 s was employed. The microhardness, MH, value (in MPa) was calculated according to the relationship [57,58]:

$$MH = 2 \sin 68^\circ \left(\frac{P}{d^2} \right)$$

where P (in N) is the contact load and d (in mm) is the diagonal length of the projected indentation area. Diagonals were measured in the reflected light mode within 30 s of load

removal, using a digital eyepiece equipped with a Leitz computer-counter-printer. Five measurements in different parts of the films of the various samples have been performed.

3.5.3. Thermogravimetric Analysis

Thermogravimetric analysis (TGA) was performed in a Q500 equipment of TA Instruments (New Castle, DE, USA), under a nitrogen or air atmosphere at different heating rates: 2, 5, 10, and 20 °C/min. The degradation temperatures of the distinct materials are determined, as well as the exact MCM-41@Irganox 1076 amount incorporated into the extruded composites, which has been estimated as an average of the values obtained from the two environments.

3.5.4. Determination of Additives by GC/MS

The additives content was determined using dichloromethane as an extraction solvent in a Soxhlet for 8 h. The extracted solution was concentrated in a rotary evaporator. The obtained residue was transferred to a chromatographic vial and dried with a nitrogen flow. Then, it was re-dissolved in a specific volume of dichloromethane. Analytical determination was carried out using a Hewlett Packard 6890 HRGC gas chromatograph equipped with an Agilent Technologies mass spectrometry detector model 5973 (Beijing China). The separation of the compounds was performed on a DB5-HT capillary column (15 m × 250 µm and 0.1 µm). The carrier gas used was helium with a flow rate of 1 mL/min. The electronic impact (70 eV) was the selected type of ionization for the mass spectrometer. The chosen chromatographic method lasted 37.5 min. The program started at 80 °C and, then, the temperature was increased at a constant rate of 8 °C/min up to 340 °C, being maintained for 5 min at that high temperature. The chromatographic protocol was chosen according to previous investigations [59].

3.5.5. Oxidation Induction Time Tests (OIT)

The oxidation induction time (OIT) was analyzed in a Mettler Toledo DSC822e differential scanning calorimeter (Columbus, OH, USA). Samples of about 5 mg were deposited in open aluminum pans, heated up to 180 °C at a rate of 20 °C/min under a nitrogen atmosphere, and maintained at that temperature for 3 min. Then, the purge gas was commuted to oxygen and the dependence of the heat flow was recorded over time, starting from the switch on to the oxidant atmosphere. The OIT value was estimated from the time of the oxidation process onset.

4. Conclusions

The functionalized particles, based on mesoporous MCM-41 silica with Irganox 1076, have been prepared by two different protocols: direct contact (MCMA particles) and a wet impregnation route with dichloromethane (MCMAD ones). These particles were further incorporated into a material containing virgin PP and a 30 wt.% of recycled PP with the purpose of guaranteeing thermal stability during its next service life. A summary of the main conclusions of the present research is as follows:

- The synergistic action between the Irganox 1076 antioxidant and the MCM-41 particles offers a very significant increase in the thermal stability in the resulting composites, as deduced from the excellent results of OIT tests;
- The use of the wet impregnation methodology and of MCM-41 particles also allows a reduction in the consumption of other antioxidants such as Irgafos 168;
- The incorporation of PPR promotes a faster virgin PP crystallization in the resulting materials, which is even higher when hybrid MCM41@Irganox 1076 particles are added;
- Moreover, a reinforcing role is also played for these modified mesoporous silicas in the resultant systems, as deduced from the corresponding MH values.

The presented methodology constitutes a promising strategy for contributing to the circular economy, since the synergy between the Irganox 1076 antioxidant and MCM-41 parti-

cles is found to play an important role in the ultimate performance of recycled polyolefins.

Author Contributions: Conceptualization, E.B.-B., M.L.C. and E.P.; methodology, E.B.-B., R.B.-G., T.M.D.-R., P.P., E.P. and M.L.C.; software, E.P.; formal analysis, E.P. and E.B.-B.; investigation, E.B.-B., R.B.-G., T.M.D.-R., P.P., E.P. and M.L.C.; resources, E.P. and M.L.C.; writing—original draft preparation, E.B.-B. and M.L.C.; writing—review and editing, E.B.-B., R.B.-G., T.M.D.-R., P.P., E.P. and M.L.C.; supervision, E.B.-B., M.L.C. and E.P.; project administration, E.P. and M.L.C.; funding acquisition, E.P. and M.L.C. All authors have read and agreed to the published version of the manuscript.

Funding: This research was funded by MCIN/AEI/10.13039/501100011033, grant number PID2020-114930GB-I00. R. Barranco-García is recipient of a “Juan de la Cierva” contract (FJC2021-046585-I) funded by MCIN/AEI/10.13039/501100011033 and the European Union “Next Generation EU”/PRTR. The authors also acknowledge the support received from the ALBA Synchrotron Light Facility.

Data Availability Statement: Data are contained within the article.

Acknowledgments: The authors are grateful to the Characterization Service for access to the SEM and TGA facilities and to the service of the Physicochemical Characterization of Polymers for DSC and GC/MS experiments, both services at ICTP-CSIC. The authors are also grateful to the personnel of these two services for their support. The synchrotron experiments were carried out in the beamline BL11-NCD-SWEET at the ALBA Synchrotron Light Facility with the collaboration of ALBA staff, to whom the authors are grateful for their support. We thank the Armando Alvarez Group for supplying PPR.

Conflicts of Interest: The authors declare no conflicts of interest.

References

1. Velásquez, E.; Patiño Vidal, C.; Copello, G.; López de Dicastillo, C.; Pérez, C.J.; Guarda, A.; Galotto, M.J. Developing Post-Consumer Recycled Flexible Polypropylene and Fumed Silica-Based Nanocomposites with Improved Processability and Thermal Stability. *Polymers* **2023**, *15*, 1142. [[CrossRef](#)] [[PubMed](#)]
2. Aurrekoetxea, J.; Sarrionandia, M.A.; Urrutibeascoa, I.; Maspoch, M.L. Effects of Recycling on the Microstructure and the Mechanical Properties of Isotactic Polypropylene. *J. Mater. Sci.* **2001**, *36*, 2607–2613. [[CrossRef](#)]
3. Blázquez-Blázquez, E.; Díez-Rodríguez, T.M.; Pérez, E.; Cerrada, M.L. Recycling of metallocene isotactic polypropylene: Importance of antioxidants. *J. Therm. Anal. Calorim.* **2022**, *147*, 13363–13374. [[CrossRef](#)] [[PubMed](#)]
4. Mihelčič, M.; Oseli, A.; Huskić, M.; Slemenik Perše, L. Influence of Stabilization Additive on Rheological, Thermal and Mechanical Properties of Recycled Polypropylene. *Polymers* **2022**, *14*, 5438. [[CrossRef](#)]
5. Tsenoglou, C.; Kartalis, C.N.; Papaspyrides, C.D.; Pfaendner, R. Modeling the Role of Stabilizing Additives During Melt Recycling of High-Density Polyethylene. *J. Appl. Polym. Sci.* **2001**, *80*, 2207–2217. [[CrossRef](#)]
6. La Mantia, F.P.; Scaffaro, R.; Baiamonte, M.; Ceraulo, M.; Mistretta, M.C. Comparison of the Recycling Behavior of a Polypropylene Sample Aged in Air and in Marine Water. *Polymers* **2023**, *15*, 2173. [[CrossRef](#)]
7. Gijnsman, P.; Fiorio, R. Long Term Thermo-Oxidative Degradation and Stabilization of Polypropylene (PP) and the Implications for its Recyclability. *Polym. Degrad. Stab.* **2023**, *208*, 110260. [[CrossRef](#)]
8. Peham, L.; Wallner, G.M.; Grabmann, M.; Beißmann, S. Temperature dependent degradation of phenolic stabilizers and ageing behaviour of PP-R micro-specimen. *Polym. Degrad. Stab.* **2023**, *211*, 110311. [[CrossRef](#)]
9. Spatafore, R.; Pearson, T. Migration and Blooming of Stabilizing Antioxidants in Polypropylene. *Polym. Eng. Sci.* **1991**, *31*, 1610–1617. [[CrossRef](#)]
10. Saunier, J.; Mazel, V.; Paris, C.; Yagoubi, N. Polymorphism of Irganox 1076: Discovery of New Forms and Direct Characterization of the Polymorphs on a Medical Device by Raman Microspectroscopy. *Eur. J. Pharm. Biopharm.* **2010**, *75*, 443–450. [[CrossRef](#)]
11. Xu, A.; Roland, S.; Colin, X. Physico-chemical characterization of the blooming of Irganox 1076[®] antioxidant onto the surface of a silane-crosslinked polyethylene. *Polym. Degrad. Stab.* **2020**, *171*, 109046. [[CrossRef](#)]
12. Zhong, B.; Lin, J.; Liu, M.; Jia, Z.; Luo, Y.; Jia, D.; Liu, F. Preparation of halloysite nanotubes loaded antioxidant and its antioxidative behavior in natural rubber. *Polym. Degrad. Stab.* **2017**, *141*, 19–25. [[CrossRef](#)]
13. Weizman, O.; Meada, J.; Dodiuk, H.; Ophir, A.; Kenig, S. The effect of nanoparticles on the loss of UV stabilizers in polyethylene films. *Polym. Degrad. Stab.* **2022**, *195*, 109811. [[CrossRef](#)]
14. Lin, J.; Luo, Y.; Zhong, B.; Hu, D.; Jia, Z.; Jia, D. Enhanced interfacial interaction and antioxidative behavior of novel halloysite nanotubes/silica hybrid supported antioxidant in styrene-butadiene rubber. *Appl. Surf. Sci.* **2018**, *441*, 798–806. [[CrossRef](#)]
15. Pan, Q.; Wang, B.; Chen, Z.; Zhao, J. Reinforcement and antioxidation effects of antioxidant functionalized silica in styrene-butadiene rubber. *Mater. Des.* **2013**, *50*, 558–565. [[CrossRef](#)]

16. Cotea, V.V.; Luchian, C.E.; Bilba, N.; Niculaua, M. Mesoporous silica SBA-15, a new adsorbent for bioactive polyphenols from red wine. *Anal. Chim. Acta* **2012**, *712*, 180–185. [[CrossRef](#)] [[PubMed](#)]
17. Lewandowski, D.; Ruskowski, P.; Pińska, A.; Schroeder, G.; Kurczewska, J. SBA-15 mesoporous silica modified with gallic acid and evaluation of its cytotoxic activity. *PLoS ONE* **2015**, *10*, 0132541. [[CrossRef](#)]
18. Rashidi, L.; Vasheghani-Farahani, E.; Soleimani, M.; Atashi, A.; Rostami, K.; Gangi, F.; Fallahpour, M.; Tahouri, M.T. A cellular uptake and cytotoxicity properties study of gallic acid-loaded mesoporous silica nanoparticles on Caco-2 cells. *J. Nanoparticle Res.* **2014**, *16*, 2285. [[CrossRef](#)]
19. Lau, M.; Giri, K.; García-Bennett, A.E. Antioxidant Properties of Probucol released from mesoporous silica. *Eur. J. Pharm. Sci.* **2019**, *138*, 105038. [[CrossRef](#)]
20. Beck, J.S.; Vartuli, J.C.; Roth, W.J.; Leonowicz, M.E.; Kresge, C.T.; Schmitt, K.D.; Chu, C.T.-W.; Olson, D.H.; Sheppard, E.W.; McCullen, S.B.; et al. A new family of mesoporous molecular sieves prepared with liquid crystal templates. *J. Am. Chem. Soc.* **1992**, *114*, 10834–10843. [[CrossRef](#)]
21. Loganathan, S.; Jacob, J.; Valapa, R.B.; Thomas, S. Influence of linear and branched amine functionalization in mesoporous silica on the thermal, mechanical and barrier properties of sustainable poly(lactic acid) biocomposite films. *Polymer* **2018**, *148*, 149–157. [[CrossRef](#)]
22. Costa, J.A.S.; de Jesus, R.A.; Santos, D.O.; Mano, J.F.; Romao, L.P.; Paranhos, C.M. Recent progresses in the adsorption of organic, inorganic, and gas compounds by MCM-41-based mesoporous materials. *Microporous Mesoporous Mater.* **2020**, *291*, 109698–109718. [[CrossRef](#)]
23. Nakajima, H.; Yamada, K.; Iseki, Y.; Hosoda, S.; Hanai, A.; Oumi, Y.; Teranishi, T.; Sano, T. Preparation and characterization of polypropylene/mesoporous silica nanocomposites with confined polypropylene. *J. Polym. Sci. Part B Polym. Phys.* **2003**, *41*, 3324–3332. [[CrossRef](#)]
24. Campos, J.M.; Lourenço, J.P.; Pérez, E.; Cerrada, M.L.; Ribeiro, M.R. Self-reinforced Hybrid Polyethylene/MCM-41 Nanocomposites: In-situ Polymerisation and Effect of MCM-41 Content on Rigidity. *J. Nanosci. Nanotechnol.* **2009**, *9*, 3966–3974. [[CrossRef](#)] [[PubMed](#)]
25. Campos, J.M.; Lourenço, J.P.; Cramail, H.; Ribeiro, M.R. Nanostructured silica materials in olefin polymerisation: From catalytic behaviour to polymer characteristics. *Prog. Polym. Sci.* **2012**, *37*, 1764–1804. [[CrossRef](#)]
26. Huang, M.H.; Choudrey, A.; Yang, P. Ag nanowire formation within mesoporous silica. *Chem. Commun.* **2000**, *12*, 1063–1064. [[CrossRef](#)]
27. Díez-Rodríguez, T.M.; Blázquez-Blázquez, E.; Fernández-García, M.; Muñoz-Bonilla, A.; Pérez, E.; Cerrada, M.L. Antimicrobial activity and crystallization features in bio-based composites of PLLA and MCM-41 particles either pristine or functionalized with confined Ag nanowires. *Polymers* **2023**, *15*, 2084. [[CrossRef](#)]
28. Juère, E.; Kleitz, F. On the nanopore confinement of therapeutic drugs into mesoporous silica materials and its implications. *Microporous Mesoporous Mater.* **2018**, *270*, 109–119. [[CrossRef](#)]
29. Barranco-García, R.; López-Majada, J.M.; Martínez, J.C.; Gómez-Elvira, J.M.; Pérez, E.; Cerrada, M.L. Confinement of iPP crystallites within mesoporous SBA-15 channels in extruded iPP-SBA-15 nanocomposites by Small Angle X-ray Scattering. *Microporous Mesoporous Mater.* **2018**, *272*, 209–216. [[CrossRef](#)]
30. Berlier, G.; Gastaldi, L.; Ugazio, E.; Miletto, I.; Iliade, P.; Sapino, S. Stabilization of quercetin flavonoid in MCM-41 mesoporous silica: Positive effect of surface functionalization. *J. Colloid Interface Sci.* **2013**, *393*, 109–118. [[CrossRef](#)]
31. Van Speybroeck, M.; Barillaro, V.; Thi, T.D.; Mellaerts, R.; Martens, J.; Van Humbeek, J.; Vermant, J.; Annaert, P.; Van Den Mooter, G.; Augustijns, P. Ordered mesoporous silica material SBA-15: A broad-spectrum formulation platform for poorly soluble drugs. *J. Pharm. Sci.* **2009**, *98*, 2648–2658. [[CrossRef](#)] [[PubMed](#)]
32. Szewczyk, A.; Brzezińska-Rojek, J.; Ośko, J.; Majda, D.; Prokopowicz, M.; Grembecka, M. Antioxidant-Loaded Mesoporous Silica—An Evaluation of the Physicochemical Properties. *Antioxidants* **2022**, *11*, 1417. [[CrossRef](#)] [[PubMed](#)]
33. Watanabe, R.; Hagihara, H.; Sato, H. Structure-property relationship of polypropylene-based nanocomposites by dispersing mesoporous silica in functionalized polypropylene containing hydroxyl groups. Part 1: Toughness, stiffness and transparency. *Polym. J.* **2018**, *50*, 1057–1065. [[CrossRef](#)]
34. Narayan, R.; Nayak, U.Y.; Raichur, A.M.; Garg, S. Mesoporous Silica Nanoparticles: A Comprehensive Review on Synthesis and Recent Advances. *Pharmaceutics* **2018**, *10*, 118. [[CrossRef](#)] [[PubMed](#)]
35. Sing, K.S.W.; Everett, D.H.; Haul, R.A.W.; Moscou, L.; Pierotti, R.A.; Rouquerol, J.; Siemieniewska, T. Reporting physisorption data for gas/solid systems with special reference to the determination of surface area and porosity. *Pure Appl. Chem.* **1985**, *57*, 603–619. [[CrossRef](#)]
36. Donohue, M.D.; Aranovich, G.L. Adsorption Hysteresis in Porous Solids. *J. Colloid Interface Sci.* **1998**, *205*, 121–130. [[CrossRef](#)]
37. Juan, R.; Paredes, B.; García-Muñoz, R.; Domínguez, C. Quantification of PP contamination in recycled PE by TREF analysis for improved the quality and circularity of plastics. *Polym. Test.* **2021**, *100*, 107273. [[CrossRef](#)]
38. Badini, C.; Ostrovskaya, O.; Bernagozzi, G.; Lanfranco, R.; Miranda, S. Recycling of Polypropylene Recovered from a Composting Plant: Mechanical Behavior of Compounds with Virgin Plastic. *Recycling* **2023**, *8*, 62. [[CrossRef](#)]
39. Larsen, Å.G.; Olafsen, K.; Alcock, B. Determining the PE fraction in recycled PP. *Polym. Test.* **2021**, *96*, 107058. [[CrossRef](#)]

40. Barranco-García, R.; Gómez-Elvira, J.M.; Ressia, J.A.; Quinzani, L.; Vallés, E.M.; Pérez, E.; Cerrada, M.L. Variation of Ultimate Properties in Extruded iPP-Mesoporous Silica Nanocomposites by Effect of iPP Confinement within the Mesostructures. *Polymers* **2020**, *12*, 70. [[CrossRef](#)]
41. Wang, N.; Fang, Q.H.; Chen, E.F.; Zhang, J. Structure, crystallization behavior, and thermal stability of PP/MCM-41 nanocomposite. *Polym. Eng. Sci.* **2009**, *49*, 2459–2466. [[CrossRef](#)]
42. Blázquez-Blázquez, E.; Barranco-García, R.; Díez-Rodríguez, T.M.; Cerrada, M.L.; Pérez, E. Combined Effects from Dual Incorporation of ATBC as Plasticizer and Mesoporous MCM-41 as Nucleating Agent on the Isothermal Crystallization in Environmentally-Friendly Ternary Composite Systems. *Polymers* **2023**, *16*, 624. [[CrossRef](#)] [[PubMed](#)]
43. Jacob, J.; Robert, V.; Valapa, R.B.; Kuriakose, S.; Thomas, S.; Loganathan, S. Poly(lactic acid)/Polyethylenimine Functionalized Mesoporous Silica Biocomposite Films for Food Packaging. *ACS Appl. Polym. Mater.* **2022**, *4*, 4632–4642. [[CrossRef](#)]
44. Kozlov, G.V.; Beloshenko, V.A.; Alov, V.Z.; Varyukhin, V.N. Microhardness of extruded polyethylene and composites based on it. *Mater. Sci.* **2000**, *36*, 431–436. [[CrossRef](#)]
45. Slouf, M.; Pavlova, E.; Krejčíková, S.; Ostafinska, A.; Zhigunov, A.; Krzyżanek, V.; Sowinski, P.; Piorkowska, E. Relations between morphology and micromechanical properties of alpha, beta and gamma phases of iPP. *Polym. Test.* **2018**, *67*, 522–532. [[CrossRef](#)]
46. Li, R.; Zhang, Z.; Liu, W.; Pan, Y.; Ji, X. Chain microstructure of two in-reactor alloy impact polypropylene resins with same stiffness and different toughness. *J. Polym. Res.* **2023**, *30*, 364. [[CrossRef](#)]
47. Wang, N.; Zhao, C.; Shi, X.; Shao, Y.; Li, H.; Gao, N. Co-incorporation of MMT and MCM-41 nanomaterials used as fillers in PP composite. *Mater. Sci. Eng. B* **2009**, *157*, 44–47. [[CrossRef](#)]
48. Miandad, R.; Rehan, M.; Barakat, M.A.; Aburiazza, A.S.; Khan, H.; Ismail, I.M.I.; Dhavamani, J.; Gardy, J.; Hassanpour, A.; Nizami, A.-S. Catalytic Pyrolysis of Plastic Waste: Moving Toward Pyrolysis Based Biorefineries. *Front. Energy Res.* **2019**, *7*, 27. [[CrossRef](#)]
49. Marcilla, A.; Gómez-Siurana, A.; Berenguer, D. Study of the influence of the characteristics of different acid solids in the catalytic pyrolysis of different polymers. *Appl. Catal. A Gen.* **2006**, *301*, 222–231. [[CrossRef](#)]
50. Barranco-García, R.; Cerrada, M.L.; Ressia, J.A.; Vallés, E.M.; García-Peñas, A.; Pérez, E.; Gómez-Elvira, J.M. Effect of mesoporous SBA-15 silica on the thermal stability of isotactic polypropylene based nanocomposites prepared by melt extrusion. *Polym. Degrad. Stab.* **2018**, *154*, 211–221. [[CrossRef](#)]
51. Yan, Y.; Hu, C.-Y.; Wang, Z.-W.; Jiang, Z.-W. Degradation of Irgafos 168 and migration of its degradation products from PP-R composite films. *Packag. Technol. Sci.* **2018**, *31*, 679–688. [[CrossRef](#)]
52. Yang, Y.; Hu, C.; Zhong, H.; Chen, X.; Chen, R.; Yam, K.L. Effects of Ultraviolet (UV) on Degradation of Irgafos 168 and Migration of Its Degradation Products from Polypropylene Films. *J. Agric. Food Chem.* **2016**, *64*, 7866–7873. [[CrossRef](#)] [[PubMed](#)]
53. Hermabessiere, L.; Receveur, J.; Himber, C.; Mazurais, D.; Huvet, A.; Lagarde, F.; Lambert, C.; Paul-Pont, I.; Dehaut, A.; Jezequel, R.; et al. An Irgafos[®] 168 story: When the ubiquity of an additive prevents studying its leaching from plastics. *Sci. Total Environ.* **2020**, *749*, 141651. [[CrossRef](#)] [[PubMed](#)]
54. Blázquez-Blázquez, E.; Lahoz, J.; Pérez, E.; Cerrada, M.L. An Effective Package of Antioxidants for Avoiding Premature Failure in Polypropylene Random Copolymer Plastic Pipes under Hydrostatic Pressure and High Temperature. *Polymers* **2021**, *13*, 2825. [[CrossRef](#)] [[PubMed](#)]
55. Luo, K.; You, G.; Zhao, X.; Lu, L.; Wang, W.; Wu, S. Synergistic effects of antioxidant and silica on enhancing thermooxidative resistance of natural rubber: Insights from experiments and molecular simulations. *Mater. Des.* **2019**, *181*, 107944. [[CrossRef](#)]
56. Prosheva, M.; Ehsani, M.; Pérez-Martínez, B.T.; Blazevska, J.; Joseph, Y.; Tomovska, R. Dry sonication process for preparation of hybrid structures based on graphene and carbon nanotubes usable for chemical sensors. *Nanotechnology* **2021**, *32*, 215601. [[CrossRef](#)] [[PubMed](#)]
57. Baltá-Calleja, F.J. Microhardness relating to crystalline polymers. *Adv. Polym. Sci.* **1985**, *66*, 117–148. [[CrossRef](#)]
58. Crawford, R.J. Microhardness testing of plastics. *Polym. Test.* **1982**, *3*, 37–54. [[CrossRef](#)]
59. Blázquez-Blázquez, E.; Cerrada, M.L.; Benavente, R.; Pérez, E. Identification of additives in polypropylene and their degradation under solar exposure studied by gas chromatography–mass spectrometry. *ACS Omega* **2020**, *5*, 9055–9063. [[CrossRef](#)]

Disclaimer/Publisher’s Note: The statements, opinions and data contained in all publications are solely those of the individual author(s) and contributor(s) and not of MDPI and/or the editor(s). MDPI and/or the editor(s) disclaim responsibility for any injury to people or property resulting from any ideas, methods, instructions or products referred to in the content.